THE JOURNAL OF PHYSICAL CHEMISTRY B

ARTICLE

pubs.acs.org/JPCB

Understanding Optoelectronic Properties of Cyano-Terminated Oligothiophenes in the Context of Intramolecular Charge Transfer

Sandra Rodríguez González,[†] Jesús Orduna,[‡] Raquel Alicante,[§] Belén Villacampa,[§] Kari A. McGee,[∥] João Pina,[⊥] J. Seixas de Melo,[⊥] Kathryn M. Schwaderer,[#] Jared C. Johnson,[#] Brady A. Blackorbay,[#] Jacob J. Hansmeier,[#] Victoria F. Bolton,[#] Tyler J. Helland,[#] Brett A. Edlund,[#] Ted M. Pappenfus,[*,#] Juan T. López Navarrete,[*,†] and Juan Casado[*,†]

[†]Department of Physical Chemistry, University of Málaga, Campus de Teatinos s/n, 29071 Málaga, Spain

[‡]Department of Organic Chemistry, and [§]Department of Condensed Matter Physics, ICMA, University of Zaragoza-CSIC, 50009 Zaragoza, Spain

[∥]Department of Chemistry, University of Minnesota, Minneapolis, Minnesota 55455, United States

[⊥]Department of Chemistry, University of Coimbra, P3049-535 Coimbra, Portugal

[#]Division of Science and Mathematics, University of Minnesota, Morris, Minnesota 56267, United States

Supporting Information

ABSTRACT: In this paper we have prepared a new series of oligothiophenes capped with hexyl groups and a variety of strong acceptors, mainly cyanovinyl moieties. An exhaustive analysis of the absorption, photophysical, electrochemical, solid state, nonlinear optical and vibrational properties has been presented guided by theoretical calculations. The investigation is centered on the efficiency of the intramolecular charge transfer (i.e., chain length and acceptor dependence) and its impact on all the relevant electronic, structural, optical, and vibrational properties. The most significant features imparted by the acceptors through the π−conjugated oligothiophene path are (i) intense visible electronic absorptions, (ii) tuned fluorescence wavelength emissions, (iii) solid state π−stacking, (iv) ambipolar redox behavior, (v) $S_1 \rightsquigarrow S_0$ internal conversion as being the major route for the deactivation of the excited state, and (vi) large electronic and vibrational contributions to their nonlinear optical response (hyperpolarizability). The analysis establishes connections between the different properties of the materials and structure−function relationships useful in organic electronics.

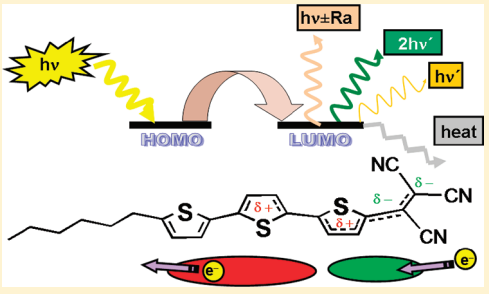

I. INTRODUCTION

Oligomers based on thiophene, or oligothiophenes, are one of the families of carbon substrates that show great promise for use as molecular semiconductors in organic electronics.[1,2] For every device application in this new field, such as OFETs (organic field effect transistors),[3] OLEDs (organic light emitting diodes),[4] OPV (organic photovoltaics) solar cells,[5] organic lasers,[6] etc., thiophene-based materials have been successfully implemented. A few reasons for the widespread application of thiophene-based oligomers include (i) their high organic synthetic versatility which provides a powerful entry for chemical design à la carte, (ii) their augmented processability in common organic solvents at room temperature, (iii) their strong chemical resistance while offering optimal π−electron delocalized systems, (iv) their very good redox properties, and (v) their tunable solid state or crystalline properties.[2] Although many oligothiophene classes are known which encompass all the applications above, even more versatile oligothiophene materials are needed to be able to surpass the important limitations still existing in the field.[2] To this end, a better understanding of structure−function relationships is required, and this paper hopes to contribute to this objective.

Recently organic solar cells have received increased attention for energy consumption reasons.[7] As for the molecular-based semiconductors in bulk heterojunction photovoltaics, cyano-based oligothiophenes, such as those prepared by Bäuerle et al.,[8,9] have become one of the most efficient families, showing promising photon-to-current conversion efficiencies. Other conjugated systems with cyano functionalizations have been also used as dye sensitizers (i.e., light absorber) in Gratzel-type solar cells.[10] Both symmetric and asymmetric cyano-based oligothiophenes have been also used as OFETs with the tetracyano-quinodimethane analogs (i.e., quinoidal oligothiophenes) showing high electron mobility and ambipolar transport.[11−15] These molecules share the common property of exhibiting intramolecular charge transfer (i.e., ICT). This feature is undoubtedly at the origin of the charge separation proccess which follows light absorption in

Received: December 23, 2010
Published: August 05, 2011

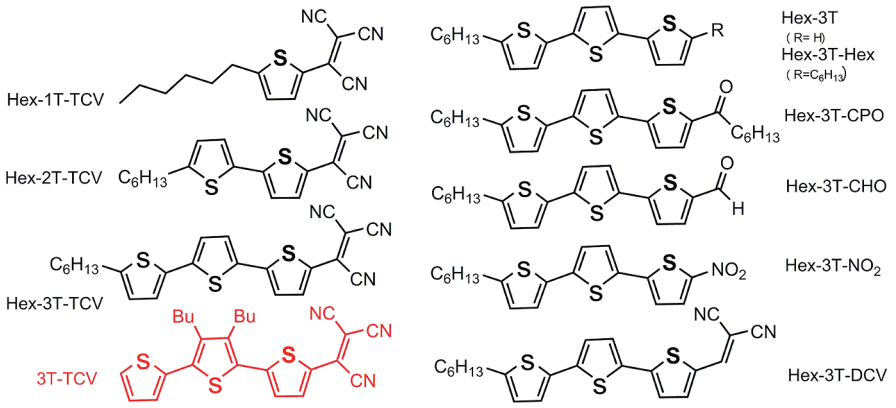

Figure 1. Chemical structures and nomenclatures of the studied compounds. The compound in red is from ref 12.

OPV devices, an effect directly related to their photovoltaic action.[7] Furthermore, it is of central importance in these devices to promote efficient charge transport of the holes and electrons to the respective electrodes. In this sense, the inclusion of saturated alkyl chains decorating the positions of the thienyl cores has been reported which has several interesting effects, for instance, (i) facilitation self-organization in solid state,[16] (ii) suppression charge recombination,[17] (iii) improvement the open-circuit voltage,[18] and (iv) enhancement the long-term stability of the solar cell (i.e., preventing water induced dye desorption from the TiO_2).[19] This paper is devoted to the study of a new set of molecules (Figure 1) possessing these chemical building blocks (i.e., oligothiophenes, cyano-based acceptors and hexyl groups) toward a better understanding of physical processes in organic materials.

Toward this end, we will describe their preparation, electronic absorption and emission properties (with emphasis on their photophysical properties), electrochemical properties, solid state morphology, nonlinear optical responses, and vibrational Raman features. Our central hypothesis establishes that their opto-electronic properties are governed by the efficiency of the donor-to-acceptor interactions which causes a ground state charge polarization and a photoinduced intramolecular charge transfer that triggers off multiple electronic events. To evaluate the molecular insights intervening in these properties, the investigation includes the parallel use of quantum chemistry in a variety of protocols (HF and TD-DFT for excited states, DFT for the vibrational Raman properties, two-state model for the NLO data, etc.).

Owing to the strong activity in the field, there is much effort in the chemical preparation and implementation of new dyes in organic devices to improve the opto-electronic features (i.e., charge mobility, luminance power, charge-to-light or photon-to-charge conversion efficiency, etc.). In order to better understand the performance of organic materials, careful analyses of the molecular (intramolecular level) events responsible for the electronic or luminescent properties are needed to put in context these device performances as well as to facilitate their comparison. In this sense, the unified understanding of the relevant phenomena affecting organic semiconductor molecules and the modeling of the main factors governing their opto-electronic properties will permit the elucidation of new and valid structure–spectroscopy relationships. This will pave the way for the realization of new organic materials with enhanced physical properties.

II. EXPERIMENTAL AND THEORETICAL METHODS

II.1. Experimental Details. UV–vis absorption spectra were recorded on a spectrophotometer Agilent 8453 instrument equipped with a diode array detection system. The spectra of the samples were recorded in solution, with spectroscopic quality solvents purchased from Sigma-Aldrich. At room temperature, dichloromethane, dimethylsulfoxide, and decaline were used, and methyltetrahydrofurane was used at 77 K. Emission spectra were measured in a FLS920P spectrofluorometer from Edinburgh Analytical Instruments (i.e., emission spectra were automatically corrected for wavelength-dependent sensitivity of the detector with standard correction curves). The fluorescence quantum yields (ϕ_F) were measured using a 1×10^{-7} mol L^{-1} quinine sulfate solution in 0.1 mol L^{-1} H_2SO_4 as the standard ($\phi_F = 0.546$). Transient triplet–triplet absorption spectra were obtained with an Applied Photophysics LKS60 laser flash photolysis apparatus pumped by a Nd:YAG laser (Spectra Physics) and using a Tektronix TDS 3052B digital analyzer. The second-order NLO properties of compounds were measured by electric field-induced second harmonic generation (EFISHG) at 1907 nm in dichloromethane. Electrochemical measurements were performed with a BAS 100B electrochemical analyzer in a C3 cell stand in a three-electrode configuration with a glassy carbon working electrode, a platinum counter electrode, and a standard Ag|AgCl|KCl (1.0 M) reference electrode using 0.1 M tetrabutylammonium hexafluorophosphate in dichloromethane as the electrolyte at room temperature. Crystallographic data were obtained on a Siemens SMART Platform CCD diffractometer at 173(2) K. Data collection was carried out using Mo Kα radiation (graphite monochromator) with a frame time of 25 s and a detector distance of 4.903 cm. FT-Raman scattering spectra were measured using a FT-Raman accessory kit (FRA/106-S) of a Bruker Equinox 55 FT-IR interferometer with a continuous-wave Nd:YAG laser source (λ_{exc} = 1064 nm). Raman spectra with the 532 nm laser excitation wavelength were recorded using a Senterra dispersive Raman microscope from Bruker. The Raman spectra were obtained with the samples as pure solids averaging 1000 scans with 2 cm^{-1} of spectral resolution. In the Supporting Information, more details are provided.

II.2. Theoretical Details. Ground state total energies, equilibrium geometries, eigenfrequencies, and normal coordinates were calculated within the framework of density functional theory (DFT)[20] by means of the Gaussian 03 package of programs.[21] Calculations were performed using Becke's three-parameter

Scheme 1. Synthesis of the Materials in This Study

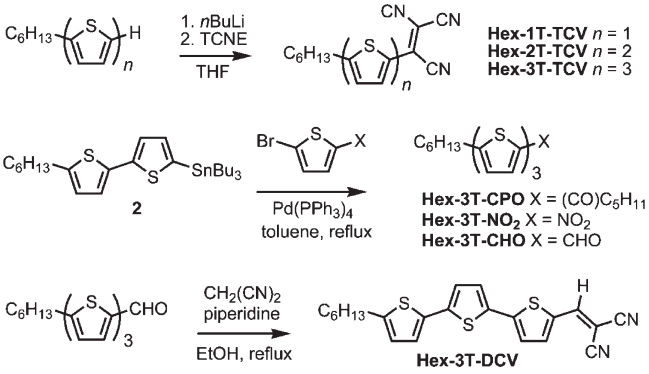

(B3) gradient-corrected exchange functional combined with the Lee−Yang−Paarr (LYP) correlation functional.[22] The coulomb-attenuating method (CAM) approximation combined with B3LYP, denoted CAM-B3LYP,[23] has been also considered since it provides significantly improved Rydberg and charge-transfer electronic excitation energies due to an improved description of the long-range exchange interaction. The 6-31G** and 6-31++G** basis sets were used.[24] For all of the DFT (including TD-DFT) data, the optimal geometries were determined on isolated-entities in gas-phase, no conformational restrictions were imposed, and inter-ring dihedral angles were freely rotatable. Theoretical Raman spectra were obtained for the resulting ground-state optimized geometries, and harmonic vibrational frequencies were corrected by a uniform factor of 0.96.[25] Raman intensities were calculated analytically and numerically. Molecular hyperpolarizabilities at zero frequency were calculated by the coupled perturbed Hartree−Fock method (CPHF).[26]

Vertical electronic transition energies and oscillator strengths were computed for the 20 lowest-energy electronic excited states, singlets and triplets, using the TDDFT approach.[27] Optimized geometries for the excited states were obtained by using the Hartree−Fock (HF) approximation by taking advantage of the restricted single excited configuration interaction approach (RCIS)[28] as incorporated in the Gaussian 03W software. For the S_1 excited state, two types of geometries were calculated: planar, with all dihedral angles between the TCV and the thiophene(s) at 180°, and perpendicular, with the dihedral angle of the TCV with the vicinal thiophene forced at 90°. The rest of geometrical parameters were freely optimized. To reproduce comparable theoretical absorption and emission spectra (Figure 4), on these HF/RCIS optimized geometries, new TD-DFT calculations have been carried out evaluating at least the ten lowest-energy vertical electronic excited states. The theoretical absorption and emission spectra of Figure 4 were obtained by convoluting the $S_0 \rightarrow S_1$ and $S_1 \rightarrow S_0$ transition energies of the HF/TD-DFT calculation with Gaussian functions (40 nm width at half-height). The relative heights of the Gaussians were determined from the oscillator strengths. All of these calculations were performed using the same 6-31G** basis set. In addition to these gas-phase calculations, and in order to explicitly take into account the solvent polarity effects, we have carried out some calculations including the effect of the solvent. Spectroscopic properties in solution were calculated using the PCM model with the overlap index between two interlocking spheres settled as 0.8 and a minimum radius of 0.5 for solvent-excluded surface spheres.[29] Decaline and DMSO were considered for the theoretical calculation with solvent effects. The same functional and basis set were used in these PCM calculations. See additional details in the Supporting Information section.

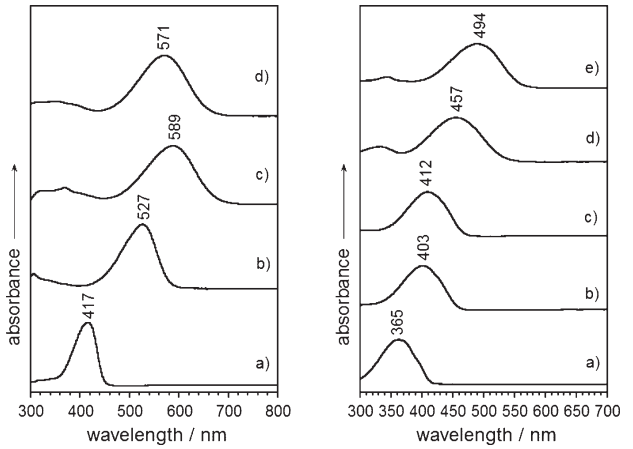

Figure 2. Left: UV−vis electronic absorption spectra in dichloromethane of (a) **Hex-1T-TCV**, (b) **Hex-2T-TCV**, and (c) **Hex-3T-TCV**, and (d) **3T-TCV**. Right: The same for (a) **Hex-3T**, (b) **Hex-3T-CPO**, (c) **Hex-3T-CHO**, (d) **Hex-3T-NO_2**, and (e) **Hex-3T-DCV**.

III. RESULTS AND DISCUSSION

III.1. Synthesis. The oligomers in this investigation were prepared according to the procedures in Scheme 1. Two main approaches exist for introducing the tricyanovinyl (TCV) functionality in conjugated oligomers: (i) the formation of organolithium species followed by quenching with tetracyanoethylene[30] and (ii) for activated aromatic rings, the addition of tetracyanoethylene (TCNE) directly to the molecule in a polar solvent.[31] The former method was used initially in the preparation of the Hex-*n*T-TCV ($n = 1-3$) series and produced compounds in low to good yields. Superior yields for **Hex-3T-TCV** were obtained via direct addition of TCNE to **Hex-3T** in DMF. This method was not applied to the monomer or dimer, however.

The majority of the remaining oligomers were prepared via Stille coupling of 5-hexyl-5′-(tributylstannyl)-2,2′-bithiophene (**2**) with the appropriate aromatic halide. The trimers prepared by this method were obtained in yields greater than 50%. Knoevenagel condensation was used to prepare **Hex-3T-DCV** utilizing a method previously reported for thiophene-dicyanovinyl materials.[32] Additional synthetic details are provided in the Supporting Information.

III.2. Absorption Spectra. Figure 2 shows the absorption spectra of the compounds in dichloromethane. The spectra of the TCV-containing molecules display broad, unresolved and active bands which show a strong red-shift of 172 nm (0.87 eV) in the **Hex-1T-TCV** → **Hex-3T-TCV** series.

Also in Figure 2 the UV−vis absorption spectra in CH_2Cl_2 are shown for the Hex-3T series, with different electron-accepting groups, which, according to the band position, are ordered by increasing wavelength. The shift in λ_{max} from **Hex-3T** → **Hex-3T-TCV** is 224 nm (1.29 eV) highlighting the electron-withdrawing effect of the acceptors over the core, the most pronounced being exerted by the tricyanovinyl group. TD-DFT/B3LYP/6-31G** and excited state calculations predict the strongest band of the spectrum of **Hex-3T-TCV** at 569 nm ($f = 0.99$)

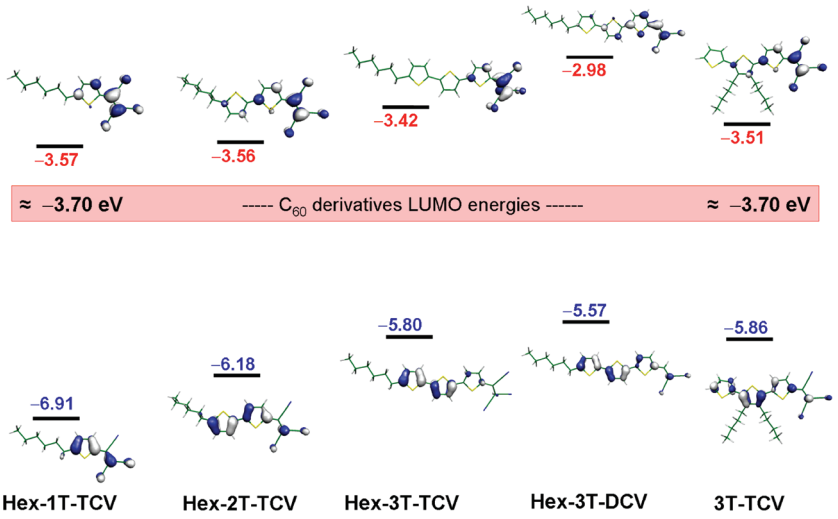

Figure 3. DFT/B3LYP/6-31G** HOMO (blue) and LUMO (red) frontier orbital energies of, from left to right, **Hex-1T-TCV**, **Hex-2T-TCV**, **Hex-3T-TCV**, **Hex-3T-DCV**, and **3T-TCV**.

which is assigned to the experimental low-lying energy band of the **Hex-3T-TCV** spectrum with a peak at 589 nm and is described as a HOMO-to-LUMO one electron transition. In order to check the accuracy of the theoretical methodology adopted, excited state calculations have been carried out by using the CAM-B3LYP functional and the more extended 6-31++G** basis set. No significant dependences with the basis sets are observed. By using CAM-B3LYP, however, excitations are overestimated. As a consequence, we can reasonably assume the B3LYP/6-31G** approach is adequate for the remaining calculations.

This assignment allows us to interpret the optical spectra as a function of their frontier orbital energies which are summarized in Figure 3. Several points are deduced: (i) The HOMO is significantly destabilized with the increasing number of thiophene rings and the LUMO is destabilized, to a lesser extent, which causes the red-shift of the optical absorption from **Hex-1T-TCV** → **Hex-3T-TCV**. (ii) In the terthiophene series, the LUMO is much more stabilized than the HOMO with the strength of the acceptor at the origin of the HOMO−LUMO and optical gap reduction in the series with variable acceptors.[33] (iii) On going from **Hex-3T-TCV** → **3T-TCV,** the HOMO and LUMO are slightly stabilized accounting for the inductive effects of unique alkyl group substitutions. (iv) Common to all of the samples is that the HOMO resides within the thienyl or oligothienyl unit whereas the LUMO resides on the acceptor group delineating an intramolecular charge transfer upon $S_0 \rightarrow S_1$ light absorption. (v) The HOMO orbitals come from the combination of the doubly occupied HOMO of the terthiophene unit and the empty LUMO of the acceptor giving rise to a ground state charge polarization. (vi) In the HOMO and LUMO orbital wave functions of **Hex-3T-TCV** and **Hex-3T-DCV**, the outermost cyano groups have a similar participation. The internal cyano of the TCV moiety, however, is greatly involved in the LUMO of **Hex-3T-TCV** yet absent in the HOMO. This can be the reason for the large 95 nm (0.40 eV) red-shift on **Hex-3T-DCV** → **Hex-3T-TCV** and tells us that this innermost cyano group strongly participates in the electronic excitation.

It is interesting to compare the LUMO energy level of our compounds with those of the electron acceptor C_{60} derivatives mostly used in organic solar cells. In a simple molecular orbital picture, such as that represented in Figure 3, the cyano-based oligothiophenes play the role of the photon capturing agents, so their intense HOMO−LUMO transition in the light absorption event locates the excited electron in the LUMO orbital from which this can be released to the empty LUMO of the acceptor at the donor−acceptor contact. As a consequence, although our approach ignores important solid state and interface effects, the comparison of the donor/acceptor LUMO orbital energies can provide a qualitative estimation of the feasibility of the electron transfer process.[8] We see that the LUMO energies of the tricyanovinyl derivatives in Figure 3 lie within 0.2 eV higher than the LUMO energies of C_{60} derivatives, whereas the difference is larger for the dicyanovinyl oligomer. This indicates that the multiple cyano substitution of the thienyl core is an interesting protocol to adjust the relevant electronic states of the donor and acceptor for charge photogeneration. This protocol has been already exploited in organic solar cells based on cyano oligothiophenes.[34]

III.3. Emission Spectra. Figure 4 displays the absorption and emission spectra of **Hex-3T-TCV** in different solvents and at variable temperature together with the theoretical absorption and emission spectra. Interestingly the emission profiles largely differ depending on the media and conditions, a feature intensively studied for many classes of oligothiophenes.[35] In the nonpolar decaline (i.e., decahydronaphthalene), the Stokes shift (measured between the spectra maxima) is around 0.13 eV, whereas in dimethylsulfoxide the shift is 0.53 eV. In addition, for the nonpolar solvent, the emission displays vibronic peaks, whereas in the polar solvent its spectrum is broad and unresolved. Our first hypothesis to explain these observations is the assumption of the presence of rotamers. As for the ground electronic state of oligothiophenes, it is well-known that this includes contributions from an ensemble of molecular conformers. Consequently one can suppose that a small fraction of molecules featuring a distortion between the terthiophene and the TCV moiety could absorb light in such a way that during the excitation-relaxation process the nuclei are kept frozen (i.e., the Born−Oppenheimer approximation).

We have simulated using theory this situation and calculated the corresponding energies and excitation parameters. There is a

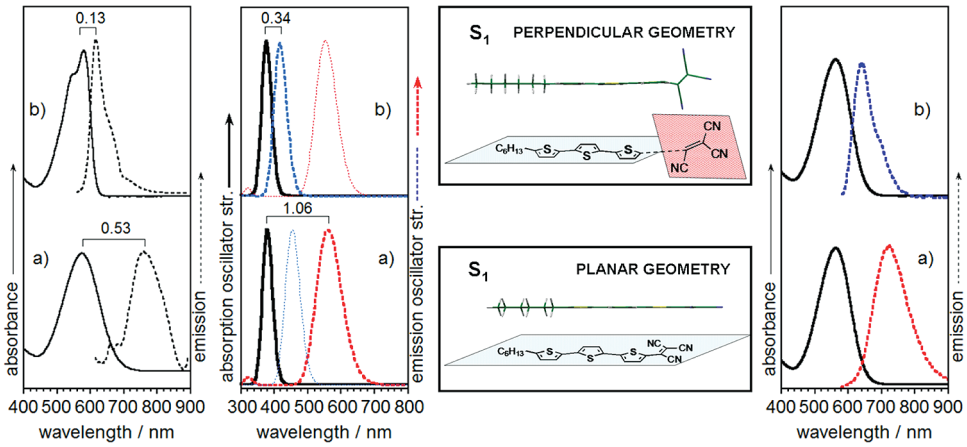

Figure 4. Spectra of **Hex-3T-TCV**: Left: (a) absorption and emission at room temperature in DMSO; (b) absorption and emission at room temperature in decaline. Right: (a) absorption and emission in methyl THF at room temperature; (b) absorption and emission in methyl THF at 77 K. Middle: HF/TDDFT/B3LYP/6-31G** spectra; Black lines: (a) absorption in DMSO and (b) in decaline with the S_0 in the planar geometry (see insert). Blue lines: (a) emission in DMSO and (b) in decaline with the S_1 having a 90° angle between the TCV and the thiophene groups, or perpendicular (see insert). Red lines: (a) emission in DMSO and (b) in decaline with the S_1 in the planar geometry.

Table 1. Spectroscopic Data (Absorption[a] and Emission[b]), Fluorescence Quantum Yields and Electrochemical[c] Potentials in Solution (Dichloromethane) at 293 K

oligomer	$\lambda_{max,abs}$ (nm)[a]	$\lambda_{max,em}$ (nm) [b]	ϕ_F (in DMSO)	ϕ_F (in CH_2Cl_2)	E^o_{ox} (V)[c]	E^o_{red} (V)
Hex-1T-TCV	417	479	0.0007	0.0002	–	−0.55, −1.43[d]
Hex-2T-TCV	527	597	0.0007	0.0005	1.73[d]	−0.48, −1.18
Hex-3T-TCV	589	750	0.0002	0.004 (0.05)	1.27, 1.64[d]	−0.47, −1.14
Hex-3T	365	419/439		0.04	1.04[d]	–
Hex-3T-CPO	403	502		0.19	1.14, 1.59[d]	−1.64
Hex-3T-CHO	412	512		0.35	1.18, 1.59[d]	−1.52
Hex-3T-NO_2	457	619		0.18	1.25, 1.63[d]	−0.94, −1.61[c]
Hex-3T-DCV	494	615		(0.02)	1.18, 1.60[d]	−1.04[c]

[a] In CH_2Cl_2. [b] In CH_2Cl_2 or toluene (in parentheses) and DMSO. [c] Potentials vs Ag/AgCl in 0.1 M $TBAPF_6/CH_2Cl_2$ solution. [d] Irreversible process. (-) E_{pa} value not provided.

good correlation of the Stokes shifts between theory and experiment including the following: (i) The more polar DMSO better stabilizes a strongly charge polarized ground electronic state and, in consequence, a very large amount of planar conformers will exist in DMSO solution. As a result, the emission is broad due to its ICT character and is displaced to the red since the planar disposition optimizes the π−electron conjugation between the 3T and TCV moieties in the excited state. (ii) The nonpolar decaline, however, imposes the opposite situation and the population of 3T/TCV twisted conformers impart the absorption and emission properties dominated by oligothienyl π-excitations, non-CT excitations.

In general, fluorescence quantum yields (ϕ_F) are very low (Table 1), and it must be noticed that ϕ_F are higher by 1 order of magnitude in the nonpolar than in the polar solvents. These data are in agreement with the Stokes shift values and also with the intramolecular charge transfer and π centered excitations generated after irradiation as discussed above.

III.4. Triplet States and Singlet Oxygen Sensitization. The triplet−triplet transient absorption spectra were obtained in toluene solution at 293 K for compounds **Hex-2T-TCV**, **Hex-3T-TCV**, and **Hex-3T-DCV** (Figure 5 and Table 2).

In addition to ground-state depletion, the transient triplet spectra show an intense absorption with bands in the range 500−800 nm. As previously observed with the unsubstituted and dicyano terminated oligothiophenes,[36] these compounds display a similar red-shift of the triplet absorption maxima with increasing number of thiophene units (going from **Hex-2T-TCV**, 620 nm, to **Hex-3T-TCV**, 700 nm) due to the increasing π−electron delocalization and intramolecular charge transfer, similar to the singlet−singlet spectra.[37] The much smaller red-shift in the triplet spectra is consistent with the strong confinement of the triplet species compared to the singlet ones.[38] From Table 2 it is seen that contrary to what was observed for the unsubstituted bithiophene and terthiophene (ϕ_T(2T) = 0.99, ϕ_T (3T) = 0.95) and dicyano terminated bi- and terthiophene[36] (ϕ_T (CN2T) = 0.97, ϕ_T(CN3T) = 0.79), the intersystem crossing quantum yields are, for the investigated compounds, significantly lower (by 1 order of magnitude). From the photophysical parameters presented in Table 2, it is clear that the internal conversion radiationless deactivation channel ($\phi_{IC} = 1 - \phi_F - \phi_{ISC}$) is responsible for the excited state deactivation of these compounds.

In an attempt to minimize internal conversion, the spectra of **Hex-3T-TCV** upon cooling are presented in Figure 4. The

dx.doi.org/10.1021/jp2070375 |J. Phys. Chem. B 2011, 115, 10573–10585

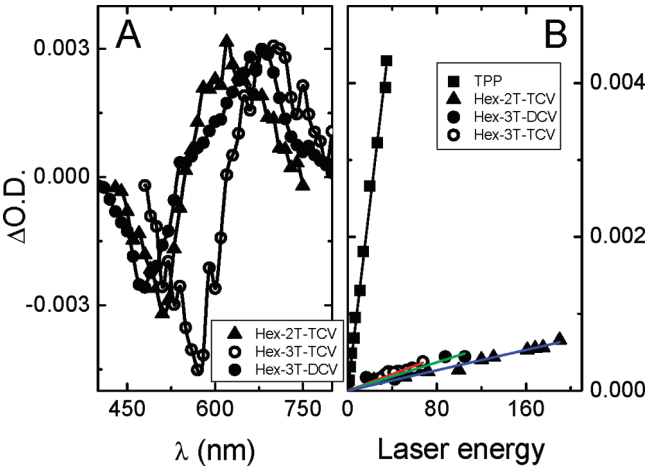

Figure 5. (A) Transient triplet−triplet absorption spectra and (B) plots of initial phosphorescence of singlet oxygen at 1270 nm as a function of laser intensity for tetraphenylporphyrin (**TPP**), **Hex-2T-TCV**, **Hex-3T-TCV**, and **Hex-3T-DCV** in toluene at 293 K.

Table 2. Spectroscopic (Triplet−Triplet Absorption Maxima and Triplet−triplet Molar Extinction Coefficients, ε_{TT}) and Photophysical Data (Intersystem Crossing Quantum Yields, ϕ_T, Sensitized Singlet Oxygen Formation Quantum Yields, ϕ_Δ, and Triplet State Decay Times, τ_T) at 293 K

oligomer	$\lambda_{max,T\text{-}T}$ (nm)	ϕ_F	ϕ_T	ϕ_Δ	τ_T (μs)	ε_{TT} (M^{-1} cm^{-1})
Hex-1T-TCV		0.0002	*a*	*b*	*a*	*a*
Hex-2T-TCV	620	0.0005	0.04	0.02	6	10400
Hex-3T-TCV	700	0.0042 (0.050)	0.04	0.03	13	8600
Hex-3T-DCV	680	(0.022)	0.08	0.02	69	18400

[a] No transient triplet−triplet absorption could be observed. [b] No singlet oxygen phosphorescence could be detected. ϕ_F see Table 1.

emission spectrum at 77 K (as in the case of the nonpolar solvent) shows a blue shift relative to the room temperature one, ruling out the presence of $T_1 \rightarrow S_0$ phosphorescence. Although intersystem crossing has been recently proposed to operate in similar intramolecular donor-to-acceptor charge transfer conjugated molecules,[39,40] it has been already mentioned (in comparison with unsubstituted oligothiophenes) that intersystem crossing in our molecules is not efficient which, in addition to the rather low optical band (i.e., in **Hex-3T-TCV** and **Hex-3T-DCV**) that favors internal conversion, can explain the absence of phosphorescence.

Alternatively singlet oxygen formation quantum yields (ϕ_Δ) from aerated solutions were also determined by plotting the initial singlet oxygen phosphorescence intensity as a function of the laser dose and comparing the slope of the curve with that obtained for tetraphenylporphyrin (TPP) as a standard (Table 2 and Figure 5B). From Table 2 it can be seen the close proximity between the ϕ_T and ϕ_Δ values, which gives support to the former values. Also, although the efficiency of triplet energy transfer to produce singlet oxygen it is not unitary ($S_\Delta = \phi_\Delta/\phi_T$), they sensitize singlet oxygen formation with a good efficiency (S_Δ = 0.29−0.68) although $T_1 \rightarrow S_0$ photon emission is unable to compete with internal conversion. The role of triplet species in the dissociation of excitons, or in the charge recombination, is known to play a role in the overall mechanism in OPVs and OLEDs devices, for instance, in the sensitizing process with C_{60} or PCBM.[8]

III.5. Electrochemical Properties. Figure 6 displays the cyclic voltammograms of some of the relevant compounds in our study, and Table 1 summarizes the electrochemical potentials. In the TCV series, **Hex-3T-TCV** and **Hex-2T-TCV** show two reversible one electron reductions at very similar potentials indicating that the LUMO in the two molecules is essentially located in the TCV moiety. Although a stable anion radical is formed in **Hex-1T-TCV**, the dianion is unstable on the CV time scale. In **Hex-2T-TCV** the first oxidation potential is irreversible being displaced at lower values in **Hex-3T-TCV** which becomes reversible. No oxidation is observed for **Hex-1T-TCV** under the experimental conditions, consistent with the large stabilization of its HOMO level (vide supra).

The electrochemical data illustrates the strong dependence of the oxidation potential with the number of thiophene rings since the HOMO completely covers the thienyl moiety. Only in the case of **Hex-3T-TCV** the ambipolar redox behavior observed is reversible which results from a fine balancing effect between the donor and the acceptor in the conjugated path. Also in **Hex-3T-CHO**, **Hex-3T-CPO**, **Hex-3T-NO_2**, and **Hex-3T-DCV**, ambipolar redox behavior is detected though the electrochemical band gaps are larger compared to **Hex-3T-TCV** consistent with the acceptor electron-withdrawing strength. Oxidations in these terthiophene compounds are very similar while reduction potentials vary depending on the acceptor: −1.52 V in **Hex-3T-CHO**, −1.64 V in **Hex-3T-CPO**, −0.94 V in **Hex-3T-NO_2**, and −1.04 V in **Hex-3T-DCV**. When **Hex-3T-DCV** and **Hex-3T-TCV** are compared, it is deduced that the second reduction process is mostly associated with the innermost cyano group of **Hex-3T-TCV**, whereas the first added electron resides in the outmost cyano periphery of the molecule.

III.6. Solid State Properties. Figure 7 shows the crystalline structure of **Hex-3T-TCV** and the molecular bond distances measured from the X-ray data together with the molecular structure predicted at the DFT/B3LYP/6-31G** level. Theory predicts reasonably well the experimental structure taking into account that calculations consider the molecule as isolated or in the gas phase while crystal packing and intermolecular interactions play a role in the solid state.

Among the three cyano groups, theory and experiment predict the CN group closest to the thiophene to display the shortest CN distance revealing that it is minimally involved in the ground state charge polarization, however, as already seen in previous sections, plays a key role as for the intramolecular $S_0 \rightarrow S_1$ light induced charge transfer. Interestingly, the solid state packing of **Hex-3T-TCV** exists as stacks of π−dimers. Due to the effect of the strong acceptor cyano units, the molecules pack antiparallel to each other so as to accommodate the hexyl chains which are out of plane from the main backbone by about 90°. In line with the X-ray data, calculations predict the hexyl chain to lie well out of the plane defined by the thienyl core. The experimental data indicates the high conformational flexibility of this group. The antiparallel packing facilitates an excellent overlap and very little slip between molecules such as represented in Figure 8. The molecules are very flat as indicated by a least-squares plane with a deviation from planarity of 0.0530 Å also in agreement with theory that predicts the π−system to be almost planar. Also in Figure 8 strong intermolecular CN···H interactions are observed in the solid state.

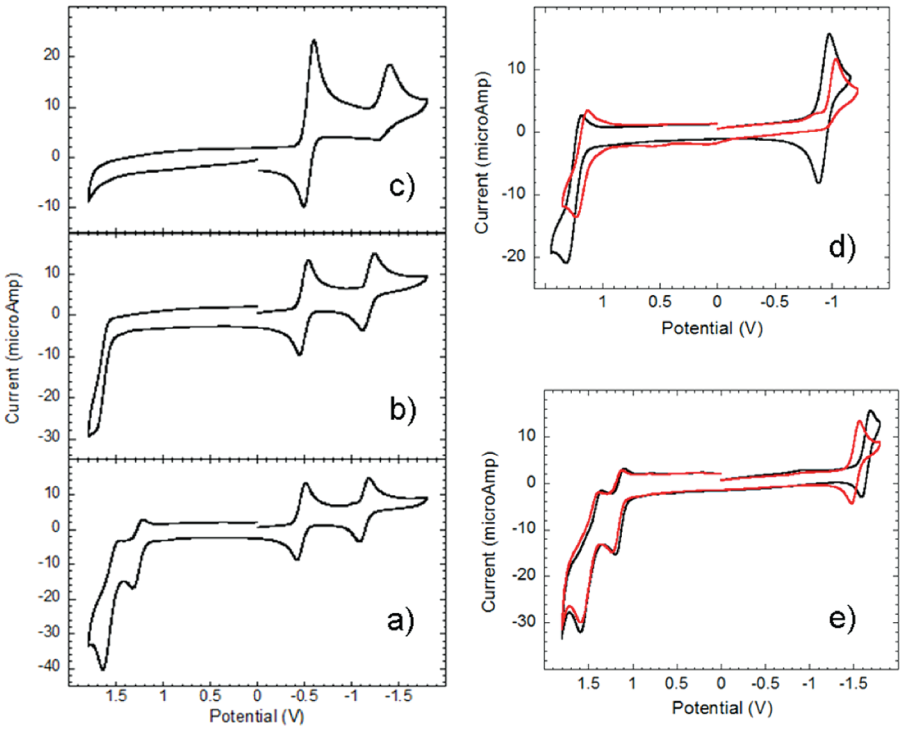

Figure 6. Electrochemical data in 0.1 M $TBAPF_6$ in CH_2Cl_2 of (a) **Hex-3T-TCV**, (b) **Hex-2T-TCV**, (c) **Hex-1T-TCV**, (d) **Hex-3T-NO_2** (black) and **Hex-3T-DCV** (red), and (e) **Hex-3T-CPO** (black) and **Hex-3T-CHO** (red).

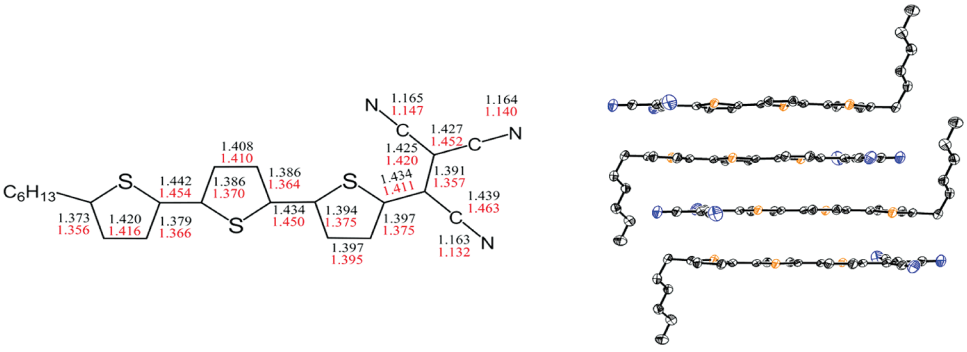

Figure 7. Left: X-ray experimental (in red) and DFT/DFT/B3LYP/6-31G** bond distances of **Hex-3T-TCV**. Right: Solid state π-stacking disposition.

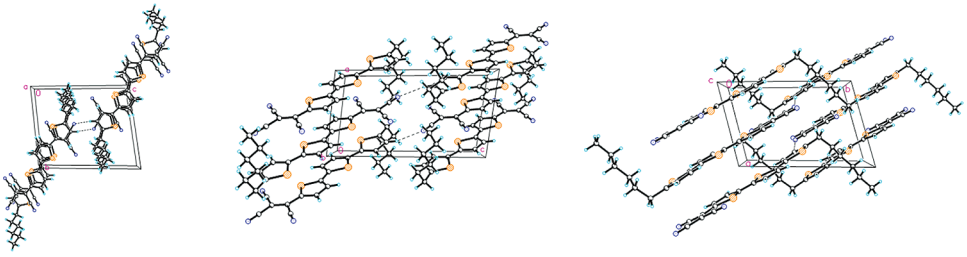

Figure 8. Different perspectives of the crystal structure of **Hex-3T-TCV**: Left: Packing diagram viewed down the *a* axis which runs along the stacks. Middle: Packing diagram viewed down the *b*-axis. Right: Packing diagram viewed down the *c* axis.

III.7. Vibrational Raman Properties. The interpretation of the vibrational Raman properties of π-conjugated materials in the framework of the effective conjugation theory (ECC) provides a satisfactory explanation of the intensity and frequency behavior of polyconjugated molecules with variable or tuned π-electron delocalization (linear π-conjugation).[41] This theory

dx.doi.org/10.1021/jp2070375 |*J. Phys. Chem. B* 2011, 115, 10573–10585

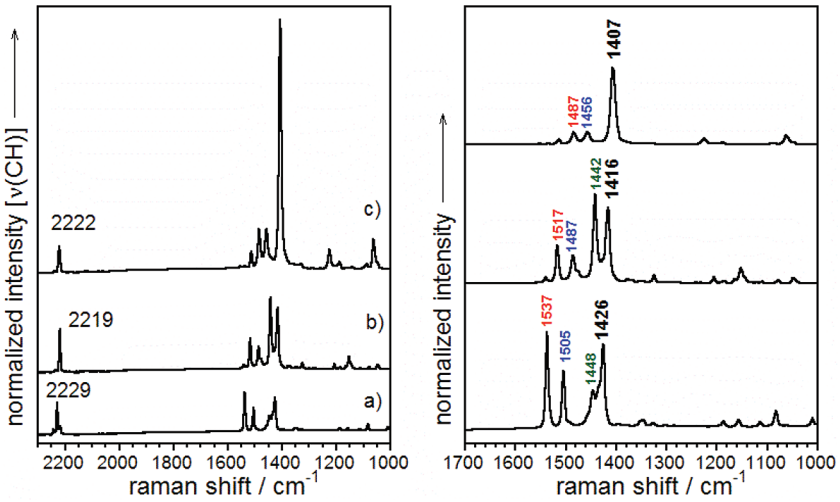

Figure 9. Left: FT-Raman spectra normalized to the $\nu(CH_2)$ stretching at 2900 cm^{-1} of (a) **Hex-1T-TCV**, (b) **Hex-2T-TCV**, and (c) **Hex-3T-TCV**. Right: The same normalizing at the strongest band.

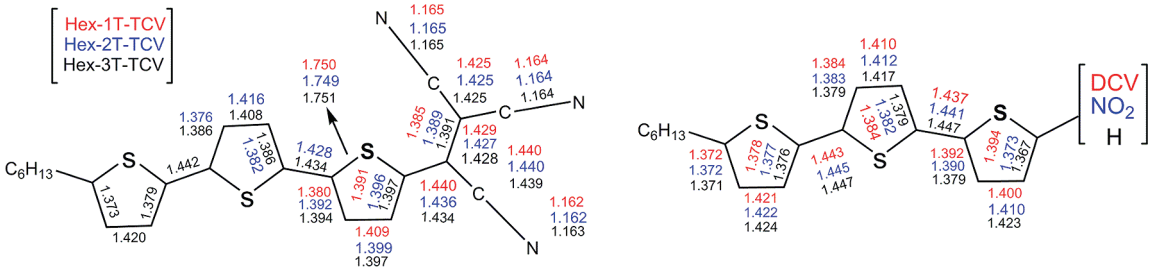

Figure 10. DFT/B3LYP/6-31G** optimized geometries of some representative molecules of this study.

states that the existence of an effective conjugation vibrational coordinate that involves the stretching and shrinking of the skeletal C═C/C−C intraring and inter-ring bonds collectively involving the delocalization of the π electrons, or ECC mode. There are two main predictions of the model: (i) the ECC mode is the strongest of the Raman spectrum showing a superlinear intensification when π-electron conjugation increases and (ii) the increasing delocalization of the π-electrons along the chain is shown by the dispersion toward lower frequencies of the ECC mode associated band or bands.

The ideal oligomeric molecules for which the model fully applies are nonsubstituted oligomers (for instance, oligothiophenes with an increasing number of thienyl units)[42] where the dynamics of the bonds bearing the conjugational effect is similar. In our push−pull molecules the inclusion of conjugated groups (i.e., acceptors) having different atoms and connectivities surely deviates from the perfect application of the model. It is interesting, however, to deduce from the spectra the ECC fingerprints and relate them with the number of thiophenes in the chain and with the electron-withdrawing power of the acceptors.

Figure 9 displays the FT-Raman spectra of the three TCV-based samples with variable chain length. The methylene groups of the hexyl chains can be considered to be sufficiently decoupled from the conjugational path to be unaffected by events involving the π electron structure. Consequently, we can evaluate the intensity evolution of π-conjugated modes by normalizing the spectra relative to the hexyl $\nu(CH_2)$ vibrational Raman bands (i.e., around 2800−2900 cm^{-1}) as shown in Figure 9.

A net intensity enhancement of the Raman spectra (i.e., C═C and C−C stretching modes) with increasing chain length is observed. As for the ν(C═C/C−C) stretching vibrations resembling the ECC modes, it is observed that among the stronger Raman lines in the three cases there are bands (same wavenumber color in the figure) that continuously downshift with the thienyl chain elongation (e.g., the lines at 1426 cm^{-1} in **Hex-1T-TCV**, 1416 cm^{-1} in **Hex-2T-TCV** and 1407 cm^{-1} in **Hex-3T-TCV**). This overall tend is nicely corroborated by quantum chemical calculations, in particular for the theoretical CC bond distances of the common thiophene (i.e., the sole thiophene of **Hex-1T-TCV** and those connected to the TCV group in **Hex-2T-TCV** and **Hex-3T-TCV**) in Figure 10 that continuously decrease (i.e., adopt more quinoidal character) as chain length increases.

For the ν(CN) stretching modes, there is a 7 cm^{-1} downshift from **Hex-1T-TCV** (2222 cm^{-1}) → **Hex-3T-TCV** (2229 cm^{-1}). This feature is in agreement with the cyano groups bearing a larger electron density as a consequence of the charge induced by the strong thienyl donor group and also with the larger quinoidal character attained on it. However the lowest ν(CN) value is unexpectedly low for **Hex-2T-TCV**. The only way to explain this result is the existence of some contribution to the ground electronic state from the charge resonance involving the closest S atom, such as is drawn in Scheme 2, or bonding character of the C−S bond in

dx.doi.org/10.1021/jp2070375 |J. Phys. Chem. B 2011, 115, 10573–10585

Scheme 2. Possible Limiting Resonant Electronic Structures Intervening in the Description of the Ground Electronic State of the TCV Molecules[a]

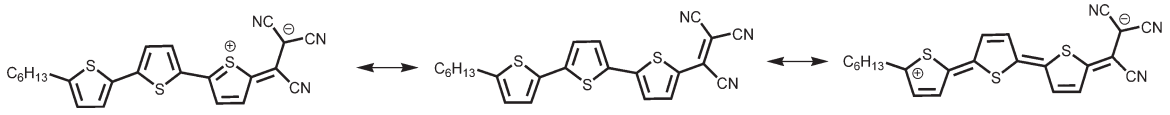

[a] The case of **Hex-3T-TCV** has been taken as an example.

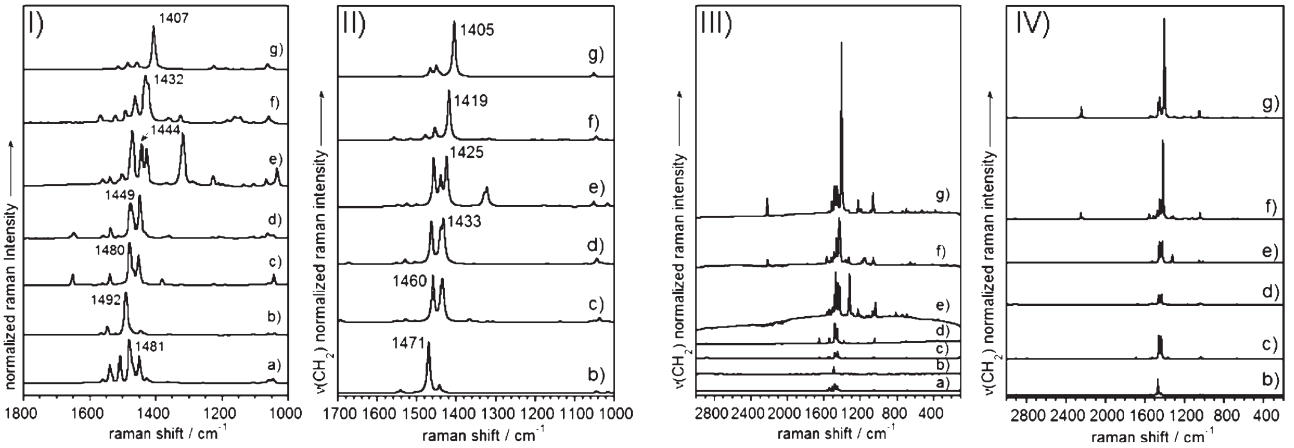

Figure 11. (I) FT-Raman spectra and (II) DFT/B3LYP/6-31G** theoretical Raman spectra, both normalized at the strongest Raman band. (III) FT-Raman spectra and (IV) DFT/B3LYP/6-31G** theoretical Raman spectra, both normalized at the $\nu(CH_2)$ stretches at 2900 cm^{-1}. The spectra correspond to (a) **Hex-3T**, (b) **Hex-3T-Hex**, (c) **Hex-3T-CHO**, (d) **Hex-3T-CPO**, (e) **Hex-3T-NO_2**, (f) **Hex-3T-DCV**, and (g) **Hex-3T-TCV**.

Hex-2T-TCV (this contrasts with the nonbonding character in the other cyano derivatives). This resonant form, although not being the dominant one, would create an excess of electron charge on the TCV moiety when overlapped with that coming from the conjugated C═C/C−C path. Support for this rationale is the involvement of the S atom closest to the TCV group in the LUMO orbital of **Hex-2T-TCV**, a configuration absent in the other two derivatives. As a consequence of this effect, the shortest CS bond distance is calculated in **Hex-2T-TCV** (1.749 Å).[43]

Figure 11 shows the FT-Raman spectra of all terthiophenes where the ECC mode is assigned as follows: 1492 cm^{-1} in **Hex-3T-Hex** (the frequency of the symmetric derivative is noted in order to conserve the dynamical effect of terminal α,disubstitution), 1480 cm^{-1} in **Hex-3T-CHO**, 1449 cm^{-1} in **Hex-3T-CPO**, 1444 cm^{-1} in **Hex-3T-NO_2**, 1432 cm^{-1} in **Hex-3T-DCV**, and 1407 cm^{-1} in **Hex-3T-TCV**. In the case of **Hex-3T-NO_2**, the assignment of the ECC mode does not correspond to the most intense Raman band of the spectrum which is due to the $\nu(C-NO_2)$ band at 1319 cm^{-1}. Also in Figure 11 the DFT/B3LYP/6-31G** theoretical Raman spectra are displayed which also shows a continuous frequency downshift of the most active Raman band by 66 cm^{-1}, relatively close to the 85 cm^{-1} shift of the ECC mode in the experimental spectra. The continuous frequency downshift of the ECC mode with the strength of the acceptor group is a consequence of the increasing quinoidal character within the thiophene rings for stronger acceptors that nicely follows the predictions of the ECC theory which is also reflected in the theoretical DFT/B3LYP/6-31G** geometries. Figure 10 shows these DFT/B3LYP/6-31G** optimized geometries of a few representative cases (e.g., DCV, NO_2, and H substitution). It is predicted that the inclusion of the acceptors transforms the heteroaromatic structures of the thiophene rings into partially heteroquinoid depending on the electron-withdrawing strength. These geometrical changes describe the molecular structure compatible with the most efficient intramolecular charge transfer going over the π-conjugational bridge. As a result, the following can be highlighted: (i) the quinoidization of the structure is greater in the cases with more powerful acceptors and (ii) the ring directly connected to the acceptor (for instance in **Hex-3T-TCV**) displays almost bond length equalization (i.e., proquinoidal character) while the outermost ring still keeps the heteroaromatic profile.

Also in Figure 11 the experimental and the DFT/B3LYP/6-31G** theoretical Raman spectra of the terthiophene molecules with the Raman intensity and theoretical activity normalized to those of the $\nu(CH_2)$ aliphatic stretching vibrations are represented. A superlinear enhancement of the ECC mode intensity is observed according to the statement of the ECC theory and also reaffirming the evolution of the conjugation efficiency in the series.

It turns out that the most powerful tricyanovinyl acceptor displays the most intense ECC mode, whereas the **Hex-3T-Hex** pair shows the lowest ECC intensity. This intensity enhancement might be ascribed to a nonlinear effect and can be considered as the vibrational portion (i.e., contribution) of the whole molecular hyperpolarizability.[44,45] In fact, the theoretical Raman activity considered as the dependence of the molecular polarizability along the normal mode movements is theoretically evaluated with an exciting frequency of zero and consequently only accounts for the true vibrational polarizability contribution or static molecular polarizability. Instead the experimental spectra obtained with an excitation laser of 1064 nm contain the vibrational and the electronic contribution arising from the excitation laser used in the Raman experiment or the dynamic

molecular polarizability. These double contributions in the experimental spectra, in contrast to the exclusive vibrational contribution in the theoretical ones, might account for the discrepancies between the intensity and activity tendencies in the spectra in Figure 11. Conversely, the overall agreement is good indicating the large contribution of the vibrational polarizability portion in the case of push−pull molecules.[46] In this sense, as illustrated in the next section, the electronic contribution to the molecular hyperpolarizability will be studied by EFISHG and the trends of the two nonlinear components analyzed.

It is interesting to discuss the evolution of the $\nu(C{\equiv}N)$ frequencies from 2218 → 2222 cm^{-1} on going from **Hex-3T-DCV** → **Hex-3T-TCV** in order to evaluate the effect of the number of cyano groups in the same acceptor structure. In **Hex-3T-TCV**, more cyano groups share the same electron releasing effect of the same donor and consequently the electron density per-cyano moiety is lower and suggests its frequency would be higher. On the other hand, the +4 cm^{-1} shift from the dicyano to the tricyano system is relatively large compared with the −7 cm^{-1} in **Hex-1T-TCV** → **Hex-3T-TCV** which emphasizes the central role of the closer CN group regarding the ground state polarization as already discussed in previous sections in relation to the HOMO−LUMO excitation and their wave function properties. At this point Raman spectroscopy allows us to shed further light on this issue by means of the resonance Raman spectrum taken with the 532 nm laser excitation, a wavelength fulfilling the lowest energy electronic absorption of the **Hex-3T-TCV**. Figure 12 displays the notable differences between the 1064 nm nonresonant Raman spectrum and the 532 nm resonant Raman spectrum of the tricyanovinyl terthiophene: while the nonresonant spectrum only shows one $\nu(C{\equiv}N)$ band at 2222 cm^{-1}, its 532 nm resonant Raman signal displays the same 2222 cm^{-1} together with a new band at higher wavenumber 2236 cm^{-1}. This new band must be assigned to the stretching mode of the innermost CN group which is largely involved in the $S_0{\rightarrow}S_1$ electron promotion excited resonantly at 532 nm, already discussed in section II.1. This result is in agreement with this CN group representing the shortest (i.e., 1.162−1.163 Å in Figure 10) CN distance among the three cyano groups indicating that it participates in the electronic transition but does not play any role as far as the ground-state charge polarization phenomenon is concerned.

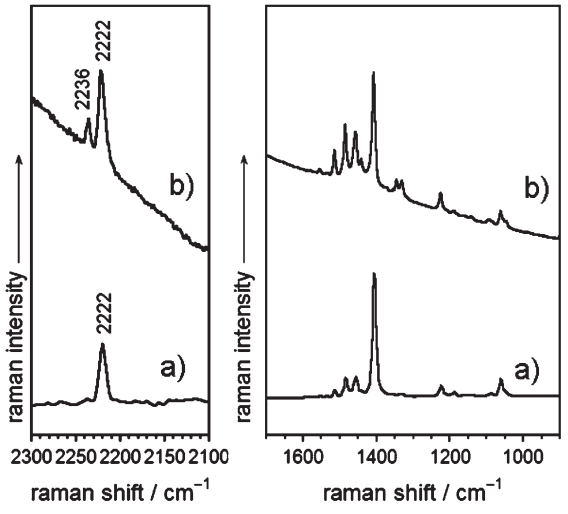

Figure 12. Left: Solid state (a) 1064 nm FT-Raman spectrum and (b) 532 nm resonant Raman spectrum of **Hex-3T-TCV**.

III.8. Nonlinear Optical Properties. Table 3 summarizes the nonlinear $\mu\beta$ values obtained from EFISHG experiments along with the values calculated for $\mu\beta(0)$ and the parameters involved in the two-state approach. As for the experimental EFISHG values, there is a straightforward correlation between the efficiency of the intramolecular charge transfer and the nonlinear $\mu\beta$ value that can be intuitively explained on the basis of the two-state approach that indicates most of the nonlinear optical response depends on the lowest energy charge-transfer transition as described by the following equation:[47]

$$\beta(0) \propto \frac{{\mu_{01}}^2 \Delta\mu_{01}}{{E_{01}}^2}$$

with $\beta(0)$ being the zero frequency molecular hyperpolarizability, E_{01} the excitation energy, μ_{01} the transition dipole moment, and $\Delta\mu_{01}$ the dipole moment change associated to this electronic transition.

As a result, and in order to provide a high $\mu\beta$ value, the topology of the orbitals mainly involved in the relevant electronic transition (i.e., the S_0 → S_1 in the two state model) should overlap along the conjugated path to yield a high transition

Table 3. Electronic Absorption Maxima and Nonlinear $\mu\beta$ Data from EFISHG at 1907 nm for Some of the Studied Compounds

	experimental			theoretical			
compounds	λ_{abs}[a]	$\mu\beta$[a,b]	$\mu\beta(0)$[b,c]	E_{01}(eV)[d]	$\Delta\mu_{01}$(D)[d]	μ_{01}(D)[d]	$\mu\beta(0)$[b,e]
Hex-1T-TCV	417 (2.97)	90	70	3.34	6.6	6.6	182
Hex-2T-TCV	527 (2.35)	650	420	2.61	15.2	9.3	983
Hex-3T-TCV	589 (2.11)	1620	905	2.18	26.3	11.0	2485
Hex-3T-CPO	403 (3.08)	*b*	*b*	2.91	13.4	9.9	129
Hex-3T-CHO	412 (3.01)	100	80	2.90	13.6	9.4	203
Hex-3T-NO_2	457 (2.71)	300	220	2.68	22.2	9.0	542
Hex-3T-DCV	494 (2.51)	470	320	2.47	20.1	11.1	1129
Hex-3T-TCV	589 (2.10)	1620	905	2.18	26.3	11.0	2485
3T-TCV	571 (2.17)	1460	850	2.27	33.7	9.7	1508

[a] In CH_2Cl_2 (x 10^{-48} esu; experimental uncertainty ±15%). [b] EFISHG signal under the experimental resolution. [c] Calculated using the two level model. [d] TD-B3LYP/6-31G** calculation. [e] HF/6-31G** calculation.

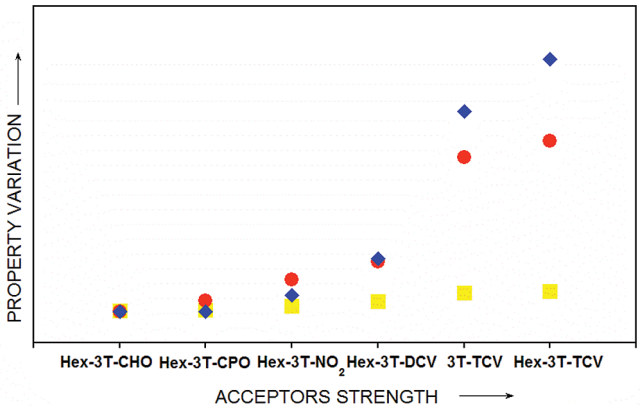

Figure 13. Representation of the normalized absorption maxima (section III.1, yellow squares), ECC Raman intensity (section III.5, blue rhombus) and EFISHG $\mu\beta$ data (section III.6, red circles). The data represented are normalized dividing by the smallest value of the series: for example in absorption, dividing by 403; in the $\mu\beta$ data dividing by 100 (for Hex-3T-CPO the normalized value is considered 1). In the Raman data, it is considered the height at the maximum of the ECC peak.

dipole moment, a requirement which is clearly attained in the tricyanovinyl substituted terthiophenes (see Figure 3 and S1 for the molecular orbitals).[48] While theoretical calculations clearly overestimate the nonlinear optical properties of the studied compounds, they provide a good qualitative prediction of the experimental trends. For example, **Hex-3T-DCV** and **Hex-3T-NO$_2$** show similar trends in the behavior of the absorption spectra, nonlinear EFISHG results and Raman data (frequencies and intensity). The extension of the oligothiophene spacer along the series **Hex-1T-TCV**, **Hex-2T-TCV**, and **Hex-3T-TCV** gives rise to increased dipole moment changes and transition dipoles and decreased excitation energies that are responsible for the large enhancement of the nonlinear optical response. The addition of one cyano group on going from **Hex-3T-DCV** to **Hex-3T-TCV** results in a 4-fold $\mu\beta$ increase, in agreement with the greater acceptor strength that gives rise to a lower E_{01} as a consequence of reduced HOMO−LUMO gap and to an increased dipole moment change on excitation. There exists a subtle role of the hexyl chains (i.e., comparing **3T-TCV** and **Hex-3T-TCV**) producing a larger $\mu\beta$ value, that according to TD-DFT calculations arises mainly from a larger transition dipole moment.

The discussion of the data is finished with Figure 13 which compares the wavelength of the absorption maxima, the $\mu\beta$ EFISHG data, and the strongest ECC band Raman intensities. The nonlinear data and the Raman intensities share the same physical phenomenon based on the hyperpolarizability, with the former providing the electronic contribution and the Raman activity evaluating the vibrational portion of it. Nonetheless, it is evident that an increase of the nonlinear behavior or superlinear enhancement occurs with the inclusion of tricyanovinyl groups.

IV. CONCLUSIONS

In this investigation we have prepared a new set of molecules based on the inclusion of hexyl groups and a variety of acceptors in thiophene-based oligomers. Given the inclusion of the cyanovinyl groups in a variety of material applications, much effort has been devoted to shed light on their role in π-conjugated systems. An exhaustive analysis of the absorption, emission, photophysics, electrochemical, solid state, and vibrational properties has been presented guided by theoretical calculations and accounted for in the context of intramolecular charge transfer. We have also documented its dependence with the oligomer chain length, with the electron-withdrawing power of the acceptor and unraveled the role of the alkyl substitution. The hexyl group exerts a moderate effect on the conjugational properties (i.e, positive inductive effect), a great beneficial impact on the processability (i.e., solubility) and in **Hex-3T-TCV** promotes π-stack arrangements which would be beneficial for charge transport.

The central effect of the intramolecular charge transfer is reflected in all the cases analyzed: i) It determines the sample color and absorptivity; ii) It promotes the detection of double emission (i.e., fluorescence) either from a planar or a twisted state; iii) The presence of the thienyl donor and CN acceptor pair confers ambipolar redox behavior, a very interesting electrochemical property pursuing ambipolar p-n conduction; iv) Evidence of $S_1 \sim\sim\rightarrow S_0$ internal conversion as being the major route for the deactivation of the excited state (with more than 99% of the quanta loss through this channel); v) The vibrational properties also reflect the efficiency of the intramolecular charge transfer both in the intensity and in the frequency behavior. This represents a rare example of the ability to correlate Raman intensity and electron-withdrawing effects within a common π-conjugated backbone; vi) The nonlinear optical properties also complement the aforementioned studies by measuring the electronic contribution to the hyperpolarizability while the Raman intensity allows for an evaluation of the vibrational portion.

Summing up, we present an incisive understanding of the optoelectronic properties in a set of new thienyl-cyano acceptor molecules. The analysis establishes connections between molecular, electronic, optical, and solid state properties, relationships which can be of interest for improving the design of new organic molecules for organic electronics.

■ ASSOCIATED CONTENT

Supporting Information. Additional spectroscopic, synthetic, photophysical, and computational details are provided. This material is available free of charge via the Internet at http://pubs.acs.org.

■ AUTHOR INFORMATION

Corresponding Author

*To whom correspondence should be addressed. E-mail: casado@uma.es.

■ ACKNOWLEDGMENT

We are indebted to the Ministerio de Ciencia e Innovación through the project references CTQ2009-10098, CTQ2008-02942, and MAT2008-06522-C02-02. S.R.G. and R.A. acknowledge the Junta de Andalucía and the BES 2006-12104 grant, respectively. The Gobierno de Aragón through the project reference E39 and the Junta de Andalucía by means of the research project PO9-4708 are also acknowledged. T.M.P. thanks the following: (i) a Grant-in-Aid of Research, Artistry and Scholarship from the Office of the Dean of the Graduate School and the Supercomputing Institute of the University of

Minnesota, (ii) University of Minnesota, Morris (UMM) Faculty Research Enhancement Funds supported by the University of Minnesota Office of the Vice President for Research and the UMM Division of Science and Mathematics for financial assistance, and (iii) the National Science Foundation (Major Research Instrumentation program through grant EAR-0722669). FCT (Portuguese Science Foundation) is acknowledged for a postdoctoral grant to J.P. (SFRH/BPD/65507/2009).

REFERENCES

(1) Roncali, J. *Chem. Rev.* **1997**, *97*, 173.Fichou, D. *Handbook of Oligo- and Polythiophenes*; Wiley-VCH: Weinheim, Germany, 1998. Baüerle, P. *Electronic Materials: The Oligomer Approach*; Müllen, K., Wegner, G., Eds; Wiley-VCH: Weinheim, Germany, 1998. Mitschke, U.; Baüerle, P. *J. Mater. Chem.* **2000**, *10*, 1471. Shirota, Y. *J. Mater. Chem.* **2000**, *10*, 1. Fichou, D. *J. Mater. Chem.* **2000**, *10*, 571. Mishra, A.; Ma, C.-Q.; Baüerle, P. *Chem. Rev.* **2009**, *109*, 1141.

(2) *Handbook of Thiophene-Based Materials: Applications in Organic Electronics and Photonics*; Perepichka, I. F., Perepichka, D. F., Eds.; Wiley: New York, 2009.

(3) Meng, H.; Zheng, J.; Lovinger, A. J.; Wang, B.-C.; Van Patten, P. G.; Bao, Z. *Chem. Mater.* **2003**, *15*, 1778. Mushrush, M.; Facchetti, A.; Lefenfeld, M.; Katz, H. E.; Marks, T. J. *J. Am. Chem. Soc.* **2003**, *125*, 9414. Facchetti, A.; Mushrush, M.; Katz, H. E.; Marks, T. J. *Adv. Mater.* **2003**, *15*, 33. Dimitrakopoulos, C. D.; Malenfant, P. R. L. *Adv. Mater.* **2002**, *14*, 99. Otsubo, T.; Aso, Y.; Takimiya, K. *J. Mater. Chem.* **2002**, *12*, 2565. Murphy, A. R.; J. Fréchet, J. M. *Chem. Rev.* **2007**, *107*, 1066.

(4) Pasini, M.; Destri, S.; Porzio, W.; Botta, C.; Giovanella, U *J. Mater. Chem.* **2003**, *13*, 807. Suzuki, M.; Fukuyama, M.; Hori, Y.; Hotta, S. *J. Appl. Phys.* **2002**, *91*, 5706. Roncali, J. *Chem. Soc. Rev.* **2005**, *34*, 483. Barbarella, G.; Favaretto, L.; Sotgiu, G.; Zambianchi, M.; Fattori, V.; Cocchi, M.; Cacialli, F.; Gigli, G.; Cingolani, R. *Adv. Mater.* **1999**, *11*, 1375. Shirota, Y.; Kinoshita, M.; Noda, T.; Okumoto, k.; Ohara, T. *J. Am. Chem. Soc.* **2000**, *122*, 11021.*Organic Light-Emitting DeVices, Synthesis, Properties, and Applications*; Müllen, K., Scherf, U., Eds.; Wiley-VCH: Weinheim, Germany, 2006.

(5) Hara, K.; Kurashige, M.; Dan-Oh, Y.; Kasada, C.; Shinpo, A.; Suga, S.; Sayama, K.; Arakawa, H. *New J. Chem.* **2003**, *27*, 783. Wang, Z.-S.; Koumura, N.; Cui, Y.; Takahashi, M.; Sekiguchi, H.; Mori, A.; Kubo, T.; Furube, A.; Hara, K. *Chem. Mater.* **2008**, *20*, 3993. Tamayo, A. B.; Walker, B.; Nguyen, T.-Q. *J. Phys. Chem. C* **2008**, *112*, 11545. Fischer, M. K. R.; López-Duarte, I.; Wienk, M. M. M.; Martínez-Díaz, V.; Janssen, R. A. J.; Baüerle, P.; Torres, T. *J. Am. Chem. Soc.* **2009**, *131*, 8669.

(6) Pisignano, D.; Anni, M.; Gigli, G.; Cingolani, R.; Zavelani-Rossi, M.; Lanzani, G.; Barbarella, G.; Favaretto, L. *Appl. Phys. Lett.* **2002**, *81*, 3534. Navarro-Fuster, V.; Calzado, E. V.; Ramirez, M. G.; Boj, P. G.; Henssler, J. T.; Matzger, A. J.; Hernández, V.; López Navarrete, J. T.; Díaz-García, M. A. *J. Mater. Chem.* **2009**, *36*, 6556.

(7) See for instante:Günes, S.; Neugebauer, H.; Sariciftci, N. S. *Chem. Rev.* **2007**, *107*, 1324. Mishra, A.; Fischer, M. K. R.; Bäuerle, P. *Angew. Chem.Int. Ed.* **2009**, *48*, 2474. Roncali, J. *Acc. Chem. Res.* **2009**, *42*, 1719.

(8) Schueppel, R.; Schmidt, K.; Uhrich, C.; Schulze, K.; Wynands, D.; Bredas, J. L.; Brier, E.; Reinold, E.; Bu, H. B.; Baüerle, P.; Maennig, B.; Pfeiffer, M.; Leo, K. *Phys. Rev. B* **2008**, *77*, 085311. Uhrich, C.; Schueppel, R.; Petrich, A.; Pfeiffer, M.; Leo, K.; Brier, E.; Kilickiran, P.; Baeuerle, P. *Adv. Func. Mater.* **2007**, *17*, 2991. Schueppel, R.; Uhrich, C.; Pfeiffer, M.; Leo, K.; Brier, E.; Reinold, E.; Baeuerle, P. *ChemPhysChem* **2007**, *8*, 1497.

(9) Very recently there is another work of dicyanovinyl oligothiophenes for photovoltaics applications: Liu, Y.; Wan, X.; Yin, B.; Zhou, J.; Long, G.; Yin, S.; Chen, Y. *J. Mater. Chem.* **2010**, *20*, 2464.

(10) Koumura, N.; Wang, Z.-S.; Mori, S.; Miyashita, M.; Suzuki, E.; Hara, K. *J. Am. Chem. Soc.* **2006**, *128*, 14256. Katoh, R.; Furube, A.; Mori, S.; Miyashita, M.; Sunahara, K.; Koumura, N.; Hara, K. *Energy Environ. Sci.* **2009**, *2*, 542. Fischer, M. K. R.; Wenger, S.; Wang, M.; Mishra, A.; Zakeeruddin, S. K.; Grätzel, M.; Bäuerle, P. *Chem. Mater.* **2010**, *22*, 1836.

(11) Casado, J.; Miller, L. L.; Mann, K. R.; Pappenfus, T. M.; Higuchi, H.; Ortiz, E.; Milian, B.; Pou-Amerigo, R.; Hernandez, V.; Lopez Navarrete, J. T. *J. Am. Chem. Soc.* **2002**, *124*, 12380. Zotti, G.; Zecchin, S.; Vercelli, B.; Berlin, A.; Casado, J.; Hernández, V.; Ortiz, R. P.; López Navarrete, J. T.; Ortí, E.; Viruela, P. M.; Milián, B. *Chem. Mater.* **2006**, *18*, 1539. Berlin, A.; Grimoldi, S.; Zotti, G.; Osuna, R. M.; Ruiz Delgado, M. C.; Ponce Ortiz, R.; Casado, J.; Hernández, V.; López Navarrete., J. T. *J. Phys. Chem. B* **2005**, *109*, 22308. Casado, J.; Zgierski, M. Z.; Ewbank, P. C.; Burand, M. W.; Janzen, D. E.; Mann, K. R.; Pappenfus, T. M.; Berlin, A.; Perez-Inestrosa, E.; Ortiz, R. P.; Lopez Navarrete, J. T. *J. Am. Chem. Soc.* **2006**, *128*, 10134. Ortiz, R. P.; Casado, J.; Hernandez, V.; Lopez Navarrete, J. T.; Viruela, P. M.; Ortí, E.; Takimiya, K.; Otsubo, T. *Angew. Chem., Int. Ed.* **2007**, *46*, 9057. Ortiz, R. P.; Casado, J.; Rodríguez González, S; Hernandez, V.; Lopez Navarrete, J. T.; Viruela, P. M.; Ortí, E.; Takimiya, K.; Otsubo, T. *Chem.—Eur. J.* **2010**, *16*, 470.

(12) Casado, J.; Ruiz Delgado, M. C.; Rey Merchán, M. C.; Hernández, V.; López Navarrete, J. T.; Pappenfus, T,M.; Williams, N.; Stegner, W. J.; Johnson, J. C.; Edlund, B. A.; Janzen, D. E.; Mann, K. R.; Orduna, J.; Villacampa, B. *Chem.—Eur. J.* **2006**, *12*, 5458.

(13) Moreno Oliva, M.; Casado, J.; Raposo, M. M. M.; Fonseca, A. M. C.; Hartmann, H.; Hernández, V.; López Navarrete, J. T. *J. Org. Chem.* **2006**, *71*, 7509.

(14) Pappenfus, T. M.; Chesterfield, R. J.; Frisbie, C. D.; Mann, K. R.; Casado, J.; Raff, J. D.; Miller, L. L. *J. Am. Chem. Soc.* **2002**, *124*, 4184. Chesterfield, R. J.; Newman, C. R.; Pappenfus, T. M.; Ewbank, P. C.; Haukaas, M. H.; Mann, K. R.; Miller, L. L.; Frisbie, C. D. *Adv. Mater.* **2003**, *15*, 1278–1282. Takahashi, T.; Matsuoka, K.; Takimiya, K.; Otsubo, T.; Aso, Y. *J. Am. Chem. Soc.* **2005**, *127*, 8928. Handa, S.; Miyazaki, E.; Takimiya, K.; Kunugi, Y. *J. Am. Chem. Soc.* **2007**, *129*, 11684. Handa, S.; Miyazaki, E.; Takimiya, K. *Chem. Commun.* **2009**, 3919.

(15) Cai, X.; Burand, M. W.; Newman, C. R.; da Silva Filho, D. A.; Pappenfus, T. M.; Bader, M.-M.; Brédas, J. L.; Mann, K. R.; Frisbie, C. D. *J. Phys.. Chem. B* **2006**, *106*, 14590. Yassar, A.; Demanze, F.; Jaafari, A.; El Idrissi, M.; Coupry, C. *Adv. Func. Mater.* **2002**, *12*, 699. Yassar, A.; Demanze, F.; Fichou, D. *Opt. Mater.* **1999**, *12*, 379.

(16) Yang, Z. Y.; Zhang, H. M.; Yan, C. J.; Li, S. S.; Yan, H. J.; Song, W. J.; Wan, L. J. *Proc. Natl. Acad. Sci. U.S.A.* **2007**, *104*, 3707.

(17) Zhang, X. H.; Wang, Z. S.; Cui, Y.; Koumura, N.; Furube, A.; Hara, K. *J. Phys. Chem. C* **2009**, *113*, 13409.

(18) Hagberg, D. P.; Yun, J.-H.; Lee, J. K.; Angelis, F. D.; Marinado, T.; Karlsson, K. M.; Humphry-Baker, R.; Sun, L.-C.; Hagfeldt, A.; Grätzel, M.; Nazeeruddin, M. K. *J. Am. Chem. Soc.* **2008**, *130*, 6259.

(19) Wang, P.; Zakeeruddin, S. M.; Moser, J. E.; Nazeeruddin, M. K.; Sekiguchi, T.; Grätzel, M. *Nat. Mater.* **2003**, *2*, 402.

(20) Stephens, P. J.; Devlin, F. J.; Chabalowski, C. F.; Frisch, M. J. *J. Phys. Chem.* **1994**, *98*, 11623.

(21) Frisch, M. J.; Trucks, G. W.; Schlegel, H. B.; Scuseria, G. E.; Robb, M. A.; Cheeseman, J. R.; Montgomery, J. A., Jr.; Vreven, T.; Kudin, K. N.; Burant, J. C.; Millam, J. M.; Iyengar, S. S.; Tomasi, J.; Barone, V.; Mennucci, B.; Cossi, M.; Scalmani, G.; Rega, N.; Petersson, G. A.; Nakatsuji, H.; Hada, M.; Ehara, M.; Toyota, K.; Fukuda, R.; Hasegawa, J.; Ishida, M.; Nakajima, T.; Honda, Y.; Kitao, O.; Nakai, H.; Klene, M.; Li, X.; Knox, J. E.; Hratchian, H. P.; Cross, J. B.; Bakken, V.; Adamo, C.; Jaramillo, J.; Gomperts, R.; Stratmann, R. E.; Yazyev, O.; Austin, A. J.; Cammi, R.; Pomelli, C.; Ochterski, J. W.; Ayala, P. Y.; Morokuma, K.; Voth, G. A.; Salvador, P.; Dannenberg, J. J.; Zakrzewski, V. G.; Dapprich, S.; Daniels, A. D.; Strain, M. C.; Farkas, O.; Malick, D. K.; Rabuck, A. D.; Raghavachari, K.; Foresman, J. B.; Ortiz, J. V.; Cui, Q.; Baboul, A. G.; Clifford, S.; Cioslowski, J.; Stefanov, B. B.; Liu, G.; Liashenko, A.; Piskorz, P.; Komaromi, I.; Martin, R. L.; Fox, D. J.; Keith, T.; Al-Laham, M. A.; Peng, C. Y.; Nanayakkara, A.; Challacombe, M.; Gill, P. M. W.; Johnson, B.; Chen, W.; Wong, M. W.; Gonzalez, C.; Pople, J. A. Gaussian 03, revision C.02; Gaussian, Inc.: Wallingford, CT, 2004.

(22) Becke, A. D. *J. Chem. Phys.* **1993**, *98*, 1372.
(23) Yanai, T.; Tew, D. P.; Handy., N. C. *Chem. Phys. Lett.* **2004**, *393*, 51.
(24) Francl, M. M.; Pietro, W. J.; Hehre, W. J.; Binkley, J. S.; Gordon, M. S.; Defrees, D. J.; Pople, J. A. *J. Chem. Phys.* **1982**, *77*, 3654.
(25) Scott, A. P.; Radom, L. *J. Phys. Chem.* **1996**, *100*, 16502.
(26) Pulay, P. *J. Chem. Phys.* **1983**, *78*, 5043. Dykstra, C. E.; Jasien, P. G. *Chem. Phys. Lett.* **1984**, *109*, 388.
(27) Runge, E.; Gross, E. K. U. *Phys. Rev. Lett.* **1984**, *52*, 997. (b) Gross, E. K. U.; Kohn, W. *Adv. Quantum Chem.* **1990**, *21*, 255.
(28) Foresman, J. B.; Head-Gordon, M.; Pople, J. A.; Frish, M. J. *J. Phys. Chem.* **1992**, *96*, 135.
(29) Tomasi, J.; Mennucci, B.; Cammi, R. *Chem. Rev.* **2005**, *105*, 2999.
(30) Pappenfus, T. M.; Burand, M. W.; Janzen, D. E.; Mann, K. R. *Org. Lett.* **2003**, *5*, 1535. Bader, M. M.; Custelcean, R.; Ward, M. D. *Chem. Mater.* **2003**, *15*, 616. Cai, C.; Liakatas, I.; Wong, M.-S.; Bosch, M.; Bosshard, C.; Gunter, P.; Concilio, S.; Tirelli, N.; Suter, U. W. *Org. Lett.* **1999**, *1*, 1847. Bu, X. R.; Li, H.; Van Derveer, D.; Mintz, E. A. *Tetrahedron Lett.* **1996**, *37*, 7331.
(31) Pappenfus, T. M.; Hermanson, B. J.; Helland, T. J.; Lee, G. G. W.; Drew, S. M.; Mann, K. R.; McGee, K. A.; Rasmussen, S. C. *Org. Lett.* **2008**, *10*, 1553. Rao, V. P.; Jen, A. K.-Y.; Wong, K. Y.; Drost, K. J. *J. Chem. Soc., Chem. Commun.* **1993**, *14*, 1118. McKusick, B. C.; Heckert, R. E.; Cairns, T. L.; Coffman, D. D.; Mower, H. F. *J. Am. Chem. Soc.* **1958**, *80*, 2806. Yoon, M.-H.; DiBenedetto, S. A.; Facchetti, A.; Marks, T. J. *J. Am. Chem. Soc.* **2005**, *127*, 1348.
(32) Nesterov, E. E.; Skoch, J.; Hyman, B. T.; Klunk, W. E.; Bacskai, B. J.; Swager, T. M. *Angew. Chem., Int. Ed.* **2005**, *44*, 5452.
(33) Casado, J; Pappenfus, T. M.; Miller, L. L.; Mann, K. R.; Ortí, E.; Viruela, P. M.; Pou-AméRigo, R.; Hernández, V.; López Navarrete, J. T. *J. Am. Chem. Soc.* **2003**, *125*, 2524.
(34) Xia, P. F.; Feng, X. J.; Lu, J.; Movileanu, R.; Tao, Y.; Baribeau, J. M.; Wong, M. S. *J. Phys.. Chem. C* **2008**, *112*, 16714.
(35) Meier, H. *Ang. Chem. Int. Ed.* **2005**, *44*, 2482. El-Gezawy, H.; Retting, W. *Chem. Phys.* **2006**, *327*, 385. Bolivar, Martinez, L. E.; dos Santos, M. C.; Galvao, D. S. *J. Phys. Chem.* **1996**, *100*, 11029. Gierschner, J.; Egelhaaf, H. J.; Mack, H. G.; Schweizer, S.; Doser, B.; Oelkrug, D. *Synth. Met.* **2003**, *138*, 311.
(36) Pina, J.; Burrows, H. D.; Becker, R. S.; Dias, F. B.; Maçanita, A. L.; Seixas de Melo, J. *J. Phys. Chem. B* **2006**, *110*, 6499.
(37) Becker, R. S.; Seixas de Melo, J.; Maçanita, A. L.; Elisei, F. *J. Phys. Chem.* **1996**, *100*, 18683.
(38) Brédas, J. L.; Cornil, J.; Beljonne, D.; dos Santos, D. A.; Shuai, Z. *Acc. Chem. Res.* **1999**, *32*, 267.
(39) Hu, J.; Xia, B.; Bao, D.; Ferreira, A.; Wan, J.; Jones, G.; Vullev, V. I. *J. Phys. Chem. A* **2009**, *113*, 3096. Bondared, S. L.; Knyukshto, V. N.; Tikhomirov, S. A.; Kalosha, I. I.; Bobrov, D. N.; Masalov, N. V.; Nevar, N. M.; Tyvorskii, V. I.; Kelin, A. V.; Kulinkovich, O. G.; Dzilinski, K. *J. App. Spectrosc.* **2002**, *69*, 230.
(40) Huss, A. S.; Pappenfus, T. M.; Bohnsack, J.; Burand, M.; Mann, K. R.; Blank, D. A. *J. Phys. Chem. A* **2009**, *113*, 10202.
(41) López Navarrete, J. T.; Zerbi, G. *J. Chem. Phys.* **1991**, *94*, 957–965. Hernández, V.; Castiglioni, C.; Del Zoppo, M.; Zerbi, G. *Phys. Rev. B* **1994**, *50*, 9815.
(42) Hernandez, V.; Casado, J.; Ramirez, F. J.; Zotti, G.; Hotta, S.; Lopez Navarrete, J. T. *J. Chem. Phys.* **1996**, *104*, 9271.
(43) Casado, J.; Zgierski, M. Z.; Hicks, R. G.; Myles, J. T.; Viruela, P. M.; Ortí, E.; Ruiz Delgado, M. C.; Hernández, V.; López Navarrete, J. T. *J. Phys. Chem. A* **2005**, *109*, 11275.
(44) Castiglioni, C.; Del Zoppo, M.; Zerbi, G. *Phys. Rev. B* **1996**, *53*, 13319.
(45) Zuliani, P.; Del Zoppo, M.; Castiglioni, C.; Zerbi, G.; Marder, S. R.; Perry, J. W. *J. Chem. Phys.* **1995**, *103*, 9935.
(46) Cho, M.; Kim, H. S.; Jeon, S. J. *J. Chem. Phys.* **1998**, *108*, 7114.
(47) Kanis, D. R.; Ratner, M. A.; Marks, T. J. *Chem. Rev.* **1994**, *94*, 195.
(48) Würthner, F.; Effenberger, F. *Chem. Phys.* **1993**, *173*, 305. Kim, O.-K.; Fort, A.; Barzoukas, M.; Blanchard-Desce, M.; Lehn, J. M. *J. Mater. Chem.* **1999**, *9*, 2227.Marder, S. R. *J. Mater. Chem.* **2009**, *19*, 40. Bourhill, G.; Brédas, J.-L.; Cheng, L.-T.; Marder, S. R.; Meyers, F.; Perry, J. W.; Tiemann, B. G. *J. Am. Chem. Soc.* **1994**, *116*, 2619.